

# Multi-objective Predictive Control of 3L-NPC Inverter Fed Sensorless PMSM Drives for Electrical Car Applications

Paul Michael Dongmo Zemgue<sup>1</sup>, Roland Christian Gamom Ngounou Ewo<sup>2</sup>, Alexandre Teplaira Boum<sup>3</sup>

<sup>1,2,3</sup> University of Douala, ENSET, Douala 1872, Cameroon

## Article Info

### Article history:

Received Feb 26, 2022

Revised Jul 25, 2022

Accepted Aug 18, 2022

### Keyword:

Multi-objective control  
Sensorless control  
Three-level inverter  
Computational load  
Cost function

## ABSTRACT

This paper proposes a multi-objective FS-MPC approach based on three-step optimization for a surface-mounted PMSM fed by a 3L-NPC inverter. It helps to significantly reduce torque ripples, current harmonics while controlling the inverter's neutral point voltage. To overcome the drawbacks of using mechanical sensors, a sliding mode observer is used to estimate the machine speed and rotor angular position. Compared to existing works, the proposed control method is implemented using the proportionality between the electromagnetic torque and the current component on the q-axis to eliminate the computational redundancy related to the current and torque control. To further reduce torque ripples and current harmonics, a 3L-NPC inverter is used. Compared to other types of three-level inverters, it uses less power semiconductors and attenuates the problem of voltage fluctuation at the neutral point and current harmonics. Matlab/Simulink simulations of the proposed approach yield a current THD of 1.69 %.

Copyright © 2022 Institute of Advanced Engineering and Science.  
All rights reserved.

## Corresponding Author:

Alexandre Teplaira Boum,  
University of Douala,  
ENSET, Douala 1872, Cameroon,  
Email: boumat2002@yahoo.fr

## NOMENCLATURE

$v_d, v_q$	Voltage in the d-q frame
$i_d, i_q$	Current in the d-q frame
$v_\alpha, v_\beta$	Voltage in the $\alpha$ - $\beta$ frame
$i_\alpha, i_\beta$	Current in the $\alpha$ - $\beta$ frame
$e_\alpha, e_\beta$	Back-EMF in the $\alpha$ - $\beta$ frame
$\omega_e$	Electrical rotor speed
$\tau$	Electrical time constant
$V_z$	Voltage at the neutral point of the inverter
DTC	Direct Torque Control
SMO	Sliding Mode Observer
FS-MPC	Finite Set Model Predictive Control
FS-PTC	Finite Set Predictive Torque Control
FCS	Finite Control Set
NPC	Neutral Point Clamped
THD	Total Harmonic Distortion
PMSM	Permanent-Magnet Synchronous motor

## 1. INTRODUCTION

The permanent magnet synchronous machine is now well established in electric vehicle drive systems, electric rail and aerospace traction and naval propulsion. Its increasing use in electric motors is due to its high power density, high efficiency and high reliability [14]. However, control of torque ripples and current harmonics is necessary to ensure proper system operation. Many control algorithms have been developed since

the proposal of DTC by Takahashi and Noguchi in [1] in 1986, the classical version of which is characterized by simplicity, fast dynamics and robustness [16]. Among these algorithms, the finite control set (FCS) algorithm based on prediction using the machine or system model takes an important place for optimal and multi-objective controls. Like any model-based control method, the FS-MPC algorithm is multi-objective since several sub-objectives can be defined for the same cost function, such as torque ripple control, stator flux control, stator current harmonic distortion control, speed control or inverter neutral point voltage control. The implementation of several sub-objectives on the same cost function creates a real computational load problem [5, 7]. The use of the three-level NPC inverter allows for a considerable reduction in current harmonics compared to the conventional inverter and also offers ease of balancing the voltages across the capacitors. However, the large number of iterations to obtain the 27 control voltage vectors increases considerably the search time for the optimal solution. Numerous works have dealt with multi-objective three-level NPC inverter controls with the target being the computational load [2-7] or the minimization of torque ripples [21, 22] by reducing the number of voltage vectors at the prediction stage [2-3], the weighting factors, the choice of which is decisive for the reliability of the control [6, 8], and the operation of the machine without angular position or speed sensors [7, 14].

To reduce the computational load, some authors prefer to reduce the number of prediction vectors. This approach impacts the number of iterations as well as the computation time of the optimal vector. Thus, [4] proposes to take into account the stator flux but also to reduce the prediction vectors. This results in a reduction of the computational complexity by the rate of 49% compared to the conventional method. In [5] the control algorithm is based on 20 fixed duty cycle modulated voltage space vectors. In [2-3] a new technique is proposed based on reducing the number of voltage vectors from 27 to 17 at the prediction stage.

Others prefer a strategic choice of the weighting factors allowing to refine the various sub-objectives of the order. The work of [6] proposes a method that consists in making an appropriate choice of the weighting factors by applying the principle of coefficient variation done online. The new cost function is constructed to target torque ripple and switching loss reduction with improved low-speed operation. It produces a reduction in the range of 29.85% to 33.33% in torque ripple and common mode voltage respectively. To further emphasize the weighting factors, [7] proposes the use of speed and current error weighting coefficients in the cost function. The resulting method performs well under steep transient conditions with a short prediction horizon and low computational load. The DC bus voltage balance is achieved by regulating the time allowed to each inverter string while they are connected to the neutral point. In this paper, [8] proposes an optimal selection of the weighting factors of the cost function based on artificial intelligence. The authors demonstrate in this scientific contribution that the proposed method can be applied not only to cost functions with multiple conflicting objectives but also to control objectives that cannot be unified without imposing an additional computational burden. On the other hand, [9] proposes a predictive torque control algorithm based on voltage vector selection that eradicates weighting factors in the cost function. This was achieved by defining only a cost function taking into account the flow error to select the optimal voltage vector in order to avoid the constant adjustment of the weighting factors. The optimization is done in two steps but the switching frequency remains variable and high. To overcome the issue of high and variable switching frequency inherent in most control algorithms, [10] proposes an algorithm that improves robustness and performance of FCS-MPC by providing "dynamic error correction" and "modified revised prediction" with reduced switching frequency.

In addition to the cost function complexity problem due to the likely large number of the control sub-objectives, which results in a long computation time for the optimal solutions, the problem of saving space for the implementation of the control system and the overall financial cost of the system remains for motorization systems. The latter is generally related to the use of encoders to read the angular position of the machine rotor in order to deduce the speed of rotation. The use of electrical speed and angle observers in the motor thus bypasses the need to obtain the rotor position via the mechanical sensor, which can reduce the reliability of the system, increase the sensitivity of the system to external disturbances and increase the financial cost of the control system [14].

In this paper, the proposed method consists of reducing the voltage vectors at the prediction stage from 27 to 19 with the objective of controlling the current, electromagnetic torque, motor speed and neutral point voltage of the 3-level NPC inverter. To avoid computational redundancy that could increase the time to find the optimal solution, the proportionality between the q-axis component of the current in the d-q frame and the electromagnetic torque of the surface-magnetized synchronous motor is exploited to control both variables. To reduce the interactions between external disturbances and the system, a sliding mode observer is used to obtain the estimated motor speed and rotor angular position. The algorithm is built on three essential steps in order to make the calculation digestible and simulated under Matlab/Simulink. A comparison of the results obtained is made with those of [3], [10], [11], [14], [19], [21] and [22].

This paper is constituted as follows: In sections 2, the research Method are presented. Sections 3 and 4 are devoted to the presentation and discussion of the results obtained under Matlab/Simulink and conclusion.

## 2. RESEARCH METHOD

### 2.1. Mathematical model of the surface-mounted PMSM

The mathematical model of the terminal voltage of the permanent magnet synchronous motor in the d-q frame is given by equation (1).

$$\begin{cases} v_d = R i_d + L_d \frac{di_d}{dt} - L_q \omega_e i_q \\ v_q = R i_q + L_q \frac{di_q}{dt} + L_d \omega_e i_d + \phi_{mag} \omega_e \end{cases} \quad (1)$$

In the d-q frame, the current, electrical speed and electromagnetic torque are given by equations (2), (3) and (4) respectively.

$$\frac{d\omega_e}{dt} = \frac{p}{J_m} \left( T_{em} - T_r - \frac{B_v}{p} \omega_e \right) \quad (2)$$

$$T_{em} = \frac{3}{2} p \left[ \phi_{mag} i_q + (L_d - L_q) i_d i_q \right] \quad (3)$$

For the surface-mounted PMSM subject to the Maximum Torque Per Ampere,  $L_d = L_q = L$  and the electromagnetic torque is proportional to the q-axis component of the d-q reference current ( $T_{em} = k_T i_q$  with  $k_T = 1,5 \cdot p \cdot \phi_{mag}$ ).

### 2.2. 3L-NPC inverter

The 3L-NPC inverter is a distributed neutral inverter topology in which loopback diodes are used to make the connection to the neutral reference point. The 3L-NPC inverters, are more popular in motor drive applications, compared to other multi-level inverter topologies [11, 20]. This topology has been studied for motor drives in several works [2-4, 16-19]. Figure 1 below shows this topology.

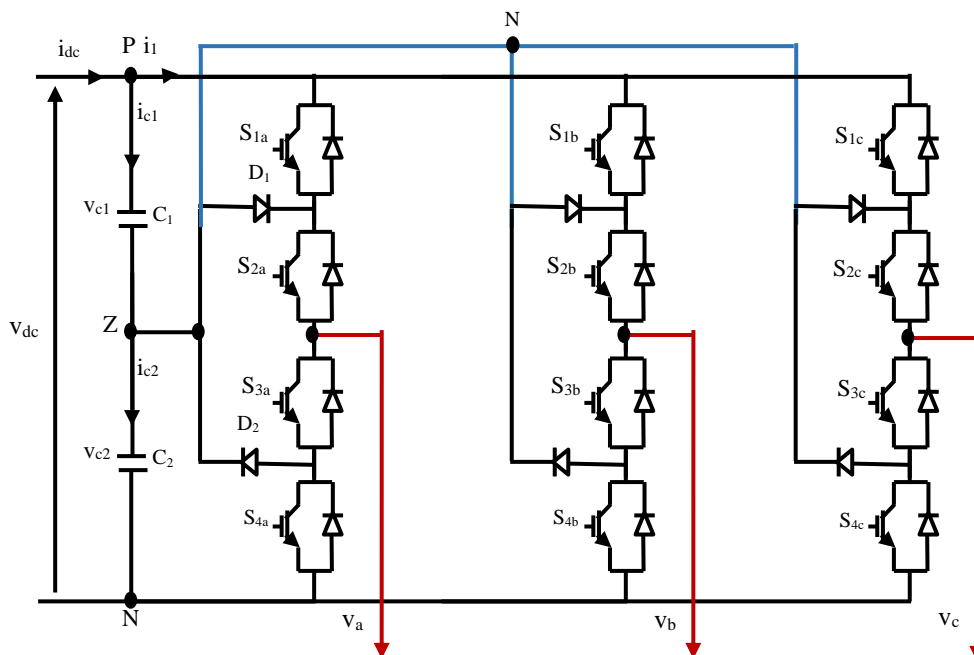


Figure 1. 3-phase NPC 3-level inverter

This inverter is made up of 12 complementary two-by-two switches and 6 clamped diodes. It allows to obtain 27 possible voltage vectors among which 18 non-redundant vectors consisting of 6 long vectors, 6 medium vectors and 6 short vectors; 8 redundant vectors and 3 null vectors as shown in the spatial distribution of figure 2 whose switch states and the voltage of one phase are given in table 1.

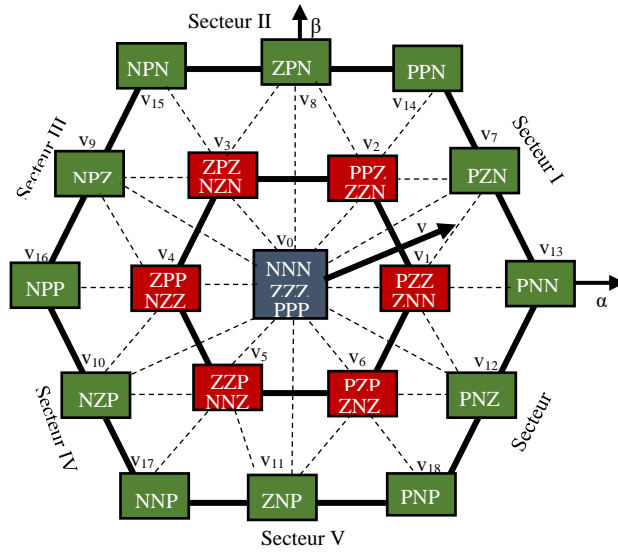


Figure 2. Voltage vector distribution of the 3-level NPC inverter

These switching states are used to synthesize the voltage vector needed to find the optimal solution.

Table 1. Presentation of the switch states and the voltage of one phase of the inverter

Switch status	Possible states				Output voltage
$S_x = a,b,c$	$S_{1x}$	$S_{2x}$	$S_{3x}$	$S_{4x}$	$V_{1x}$
P	1	1	0	0	$V_{dc}/2$
Z	0	1	1	0	0
N	0	0	1	1	$-V_{dc}/2$

Some of these switching states can produce the same voltage vector amplitude but with opposite effects on capacitor charging and discharging, which significantly affect motor performance [3].

### 2.3. Three-stage optimization based on the FS-PTC algorithm

#### 2.3.1. Proposed control scheme

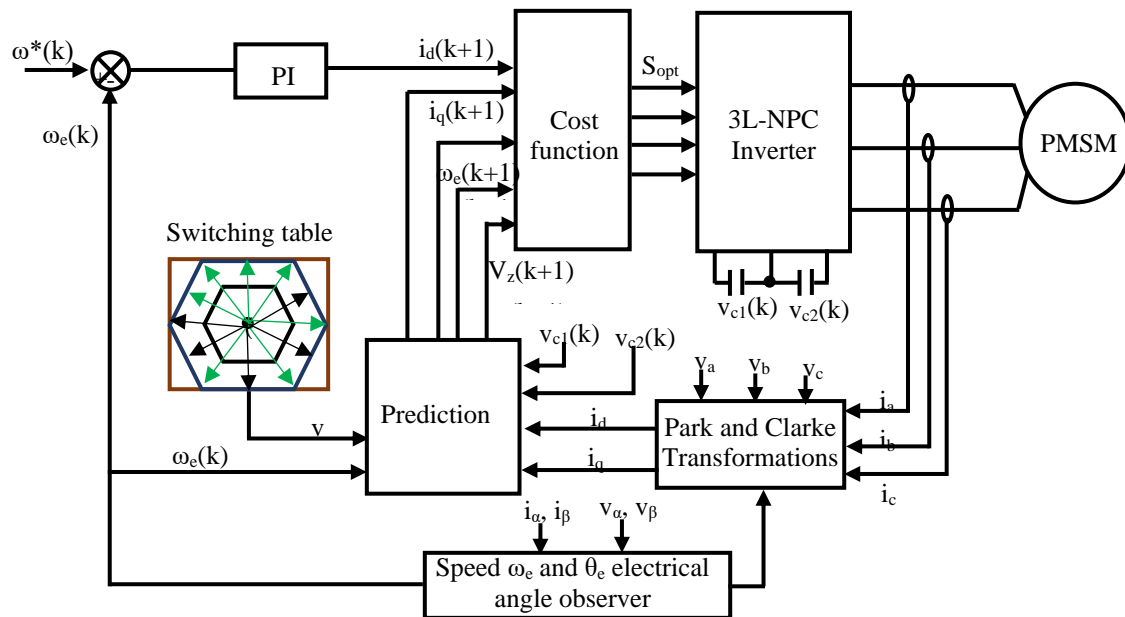


Figure 3. Proposed control scheme

The proposed three-step multi-objective FS-MPC method as shown in figure 3 consists of the following parts: estimation of speed and electrical angle by a sliding mode observer, selection of the optimal voltage vector, prediction and minimization of the cost function. The stator currents and DC bus capacitor voltages are measured while the motor speed and motor electrical angle are observed. The selection of the optimal voltage vector is performed by taking into account exclusively the 19 non-redundant vectors of the voltage space consisting of a zero vector, the 6 short vectors, the 6 medium vectors and the 6 long vectors. The control variables considered in the proposed method are current, motor speed, neutral point voltage under the constraint of overcurrent protection.

### 2.3.2. Speed and electrical angle observer

The speed and angle observer bypasses the obtaining of the rotor position via the mechanical sensor that may influence the reliability of the system due to external disturbances [14]. The model of the machine in the  $\alpha$ - $\beta$  frame of reference developed from the back-electromotive forces  $e_\alpha$  and  $e_\beta$  is defined by (4):

$$\frac{d}{dt} \begin{bmatrix} \hat{i}_\alpha \\ \hat{i}_\beta \end{bmatrix} = \frac{1}{L} \begin{bmatrix} v_\alpha \\ v_\beta \end{bmatrix} - \frac{R}{L} \begin{bmatrix} \hat{i}_\alpha \\ \hat{i}_\beta \end{bmatrix} - \frac{1}{L} \begin{bmatrix} e_\alpha \\ e_\beta \end{bmatrix} \quad (4)$$

The conventional sliding mode observer applied to the surface-mounted PMSM is described by the relation (5).

$$\frac{d}{dt} \begin{bmatrix} \hat{i}_\alpha \\ \hat{i}_\beta \end{bmatrix} = \frac{1}{L} \begin{bmatrix} v_\alpha \\ v_\beta \end{bmatrix} - \frac{R}{L} \begin{bmatrix} \hat{i}_\alpha \\ \hat{i}_\beta \end{bmatrix} - \frac{k_{SMO}}{L} \begin{bmatrix} \text{sign}(\hat{i}_\alpha - i_\alpha) \\ \text{sign}(\hat{i}_\beta - i_\beta) \end{bmatrix} \quad (5)$$

Where  $\hat{i}$  denotes the estimated values, and  $k_{SMO}$  the constant gain of the observer. The conventional SMO uses the signum function which causes the proliferation of disturbances in the system [13]. Thus the sigmoid function is preferred because of its moderate interactions with the disturbances. This sigmoid function is defined by the relation (6).

$$H(\tilde{i}) = \left[ \left( \frac{2}{1 + e^{-a\tilde{i}}} \right) - 1 \right] \text{ with } \begin{bmatrix} \tilde{i}_\alpha \\ \tilde{i}_\beta \end{bmatrix} = \begin{bmatrix} \hat{i}_\alpha - i_\alpha \\ \hat{i}_\beta - i_\beta \end{bmatrix} \quad (6)$$

Equation (7) below is obtained by substituting the signum function for the sigmoid function in equation (6).

$$\frac{d}{dt} \begin{bmatrix} \hat{i}_\alpha \\ \hat{i}_\beta \end{bmatrix} = \frac{1}{L} \begin{bmatrix} v_\alpha \\ v_\beta \end{bmatrix} - \frac{R}{L} \begin{bmatrix} \hat{i}_\alpha \\ \hat{i}_\beta \end{bmatrix} - \frac{k_{SMO}}{L} \begin{bmatrix} H(\tilde{i}_\alpha) \\ H(\tilde{i}_\beta) \end{bmatrix} \quad (7)$$

The SMO described by equation (7) is stable in the Lyapunov sense when  $k_{SMO}$  is chosen large enough, i.e.  $k_{SMO} > \max(|e_\alpha|, |e_\beta|)$  [15]. Equation (8) is obtained by applying Euler's formula to equation (7).

$$\begin{cases} \hat{i}_\alpha(k+1) = \hat{i}_\alpha(k) + \frac{T_s}{L} v_\alpha - \frac{R}{L} T_s \hat{i}_\alpha(k) - \frac{k_{SMO} \cdot T_s}{L} H(\tilde{i}_\alpha(k)) \\ \hat{i}_\beta(k+1) = \hat{i}_\beta(k) + \frac{T_s}{L} v_\beta - \frac{R}{L} T_s \hat{i}_\beta(k) - \frac{k_{SMO} \cdot T_s}{L} H(\tilde{i}_\beta(k)) \end{cases} \quad (8)$$

By posing  $\tau = \frac{L}{R}$ , the electrical time constant and  $\chi = \frac{k_{SMO} \cdot T_s}{L}$ , observer's time gain, relationship (9) is deduced.

$$\begin{bmatrix} \hat{i}_\alpha(k+1) \\ \hat{i}_\beta(k+1) \end{bmatrix} = \begin{bmatrix} 1 - \frac{T_s}{\tau} & 0 \\ 0 & 1 - \frac{T_s}{\tau} \end{bmatrix} \begin{bmatrix} \hat{i}_\alpha(k) \\ \hat{i}_\beta(k) \end{bmatrix} - \begin{bmatrix} \frac{T_s}{L} & 0 \\ 0 & \frac{T_s}{L} \end{bmatrix} \begin{bmatrix} v_\alpha \\ v_\beta \end{bmatrix} - \begin{bmatrix} \chi & 0 \\ 0 & \chi \end{bmatrix} \begin{bmatrix} H(\tilde{i}_\alpha(k)) \\ H(\tilde{i}_\beta(k)) \end{bmatrix} \quad (9)$$

By introducing the second-order identity matrix into (10), the discrete equation of the sliding-mode observer is deduced by (10).

$$\begin{bmatrix} \hat{i}_\alpha(k+1) \\ \hat{i}_\beta(k+1) \end{bmatrix} = \gamma \cdot I \cdot \begin{bmatrix} \hat{i}_\alpha(k) \\ \hat{i}_\beta(k) \end{bmatrix} - \frac{T_s}{L} \begin{bmatrix} v_\alpha \\ v_\beta \end{bmatrix} - \chi \cdot \begin{bmatrix} H(\tilde{i}_\alpha(k)) \\ H(\tilde{i}_\beta(k)) \end{bmatrix} \text{ with } I = \begin{bmatrix} 1 & 0 \\ 0 & 1 \end{bmatrix}, \begin{bmatrix} \tilde{i}_\alpha(k) \\ \tilde{i}_\beta(k) \end{bmatrix} = \begin{bmatrix} \hat{i}_\alpha(k) - i_\alpha(k) \\ \hat{i}_\beta(k) - i_\beta(k) \end{bmatrix}, \gamma = \frac{1 - T_s}{\tau} \quad (10)$$

The electrical angular position of the rotor is estimated using the negative arc tangent method based on the back-EMF. The observed electrical angular measurement of the rotor is obtained as follows:

$$\hat{\theta}_e(k) = -\arctan \left[ \frac{H(\tilde{i}_\alpha(k))}{H(\tilde{i}_\beta(k))} \right] \text{ with } \hat{\omega}_e(k) = \frac{\hat{\theta}_e(k+1) - \hat{\theta}_e(k)}{T_s}.$$

**2.3.3. Selection of the optimal voltage vector**

Figure 4 shows the voltage vector distribution of the used 3-level NPC inverter.

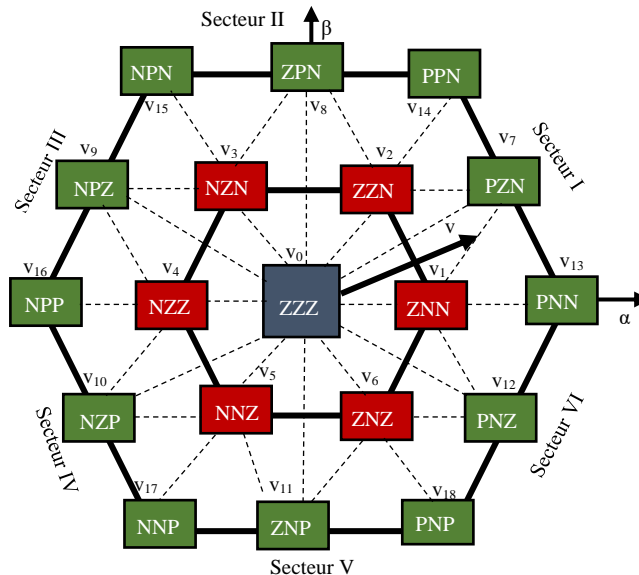


Figure 4. Distribution of the used voltage vectors

In this paper, the 18 non-redundant vectors ( $\vec{v}_1$  to  $\vec{v}_{18}$ ) and one null vector ( $\vec{v}_0$ ) are exploited to generate the optimal control sequence  $S_{opt}$ . This is done in order to reduce 8 iterations in searching for the optimal solution. Indeed, the control objectives are quadratic functions of current, speed and voltage at the neutral point of the inverter. Thus, redundant sequences of the same vector are likely to produce the same solution with the only difference that it extends the search time for the optimal solution. This reduction in the number of iterations makes it possible to exploit the trade-off between multiple objectives and the computational load. The voltage  $v_d$  and  $v_q$  used in (1) are obtained from the matrix equation (11) where  $v_\alpha$  and  $v_\beta$  are the real and imaginary parts respectively if the voltage vector whose expression is given by (12).

$$\begin{bmatrix} v_d \\ v_q \end{bmatrix} = \begin{bmatrix} \cos \theta_e & -\sin \theta_e \\ \sin \theta_e & \cos \theta_e \end{bmatrix} \begin{bmatrix} v_\alpha \\ v_\beta \end{bmatrix} \quad (11)$$

$$v = \frac{2}{3} (V_{an} + aV_{bn} + a^2V_{cn}) \text{ with } a = e^{j\frac{2\pi}{3}} \quad (12)$$

The voltage  $V_{an}$ ,  $V_{bn}$  and  $V_{cn}$  are given by table 1.

### 2.3.4. Prediction

Since the control variables of the proposed method are current, motor speed, electromagnetic torque and inverter neutral point voltage, by applying Euler's formula to equations (1), (2) and (3) above, equations (13), (14) and (15) are deduced.

$$\begin{bmatrix} i_d(k+1) \\ i_q(k+1) \end{bmatrix} = \begin{bmatrix} \gamma & T_s \omega_e(k) \\ -T_s \omega_e(k) & \gamma \end{bmatrix} \begin{bmatrix} i_d(k) \\ i_q(k) \end{bmatrix} + \begin{bmatrix} \chi & 0 \\ 0 & \chi \end{bmatrix} \begin{bmatrix} v_d(k) \\ v_q(k) \end{bmatrix} + \begin{bmatrix} 0 \\ -\varphi_{mag} \cdot \chi \cdot \omega_e(k) \end{bmatrix} \quad (13)$$

$$\hat{\omega}_e(k+1) = \hat{\omega}_e(k) + \frac{p \cdot T_s}{J_m} \left( T_{em}(k) - T_r - \frac{B_v}{p} \hat{\omega}_e(k) \right) \quad (14)$$

$$T_{em}(k+1) = k_T \cdot i_q(k+1) \quad (15)$$

The discrete equations for the voltages across capacitors  $C_1$  and  $C_2$  and their currents are given by (16) respectively:

$$\begin{cases} V_{ci}(k+1) = V_{ci}(k) + \frac{T_s}{C} i_{ci}(k) \text{ with } i = \{1, 2\} \\ \begin{bmatrix} i_{c1}(k+1) \\ i_{c1}(k+1) \end{bmatrix} = \begin{bmatrix} i_{dc} \\ i_{dc} \end{bmatrix} - \begin{bmatrix} S_{1a} & S_{1b} & S_{1c} \\ S_{2a}-1 & S_{2a}-1 & S_{2a}-1 \end{bmatrix} \begin{bmatrix} i_a(k) \\ i_b(k) \\ i_c(k) \end{bmatrix} \end{cases} \quad (16)$$

Where  $V_{ci}$  represent the voltage across capacitor  $\{1, 2\}$ ,  $i_{c1}$  the current through capacitor  $C_1$  and  $i_{c2}$  the current through capacitor  $C_2$ . The predicted voltage at the neutral point of the inverter can therefore be deduced by (17):

$$V_z(k+1) = V_z(k) + \frac{T_s}{C} [i_{c1}(k+1) - i_{c2}(k+1)] \quad (17)$$

Keeping this voltage close to 0 is essential for balanced operation of the inverter.

### 2.3.5. Cost Function

The cost function will be evaluated for the 19 states to find the best combination in the three stages. The proposed cost function for this method aims to control both the current, the electromagnetic torque, the motor speed and the voltage at the neutral point of the inverter. The proposed cost function will therefore take into account three types of errors:

- The pipe errors ( $g_1$ ) which comprise the quadratic form of the d-axis component of the current and voltage at the neutral point. This function is defined by (18).

$$g_1 = \lambda_{i_d} (i_d(k+1))^2 + \lambda_{v_z} (v_z(k+1))^2 \quad (18)$$

- The tracking errors ( $g_2$ ) which include the quadratic form of the q-axis component of current and torque. This function is defined by (19).

$$g_2 = \lambda_{i_q} \left( i_q^*(k+1) - i_q(k+1) \right)^2 + \lambda_{T_{em}} \left( T_{em}^*(k+1) - T_{em}(k+1) \right)^2 \quad (19)$$

- Restriction errors ( $g_3$ ). This function (19) is used to monitor overcurrents.

$$g_3 = I_m = \begin{cases} \sqrt{i_d^2 + i_q^2} - I_{max} & \text{if } \sqrt{i_d^2 + i_q^2} \geq I_{max} \\ 0 & \text{Otherwise} \end{cases} \quad (20)$$

Where  $\lambda_{i_d}$ ,  $\lambda_{v_z}$ ,  $\lambda_{i_q}$ ,  $\lambda_{T_{em}}$  are the weighting factors of current  $i_d$ , neutral point voltage  $V_z$ , current  $i_q$  and electromagnetic torque  $T_{em}$  respectively. As the motor is surface magnetised and the electromagnetic torque is set proportional to the current on the q-axis of the d-q frame, equation (19) becomes (21).

$$g_2 = \left( \lambda_{i_q} + k_T^2 \cdot \lambda_{T_{em}} \right) \left( i_q^*(k+1) - i_q(k+1) \right)^2 \quad (21)$$

This property of proportionality between the electromagnetic torque makes it possible to eliminate the calculation redundancy in  $g_2$  of  $\left( i_q^*(k+1) - i_q(k+1) \right)^2$  and  $\left( T_{em}^*(k+1) - T_{em}(k+1) \right)^2$  which can be reduced to the single function  $\left( \lambda_{i_q} + k_T^2 \cdot \lambda_{T_{em}} \right) \left( i_q^*(k+1) - i_q(k+1) \right)^2$ . The global objective function of the proposed control is defined by (23) :

$$g = \sum_{i=1}^3 g_i \text{ with } g_3 = \begin{cases} \sqrt{i_d^2 + i_q^2} - I_{max} & \text{if } \sqrt{i_d^2 + i_q^2} \geq I_{max} \\ 0 & \text{Otherwise} \end{cases} \quad (22)$$

### 3. RESULTS AND DISCUSSION

#### 3.1. Simulation results

To verify the effectiveness of the proposed method, simulations were carried out in the Matlab/Simulink virtual laboratory. Table 2 below shows the different parameters used in these simulations.

Table 2. Simulation parameters

Parameters	Designation	Value
R	Stator resistance	2.98 $\Omega$
L	Machine inductances	7 mH
$\Phi_{mag}$	Flux generated by the permanent magnet	0.135 Wb
$T_r$	Load torque	5 N.m
$J_m$	Moment of inertia of the machine	$0.47 \times 10^{-5}$ kg.m <sup>2</sup>
$B_v$	Viscous coefficient of friction	0.00001 N.m.s/rad
$T_s$	Sampling period	0.04 ms
p	Number of pole pairs	2
$k_{SMO}$	Observer gain	140
$V_{dc}$	DC bus voltage	270 V
$\lambda_{i_d}, \lambda_{i_q}, \lambda_{T_{em}}, \lambda_{v_z}$	Weighting factors	$10^{-4}, 2 \times 10^{-3}, 2 \times 10^{-3}, 1.5 \times 10^{-5}$
$C_1, C_2$	Capacitor $C_1$ and $C_2$	$1500 \times 10^{-3}$ F

Firstly, to study the steady state performance of the control, tests were carried out at constant speed and low load torque and then at high load torque. The electrical and observed quantities are given in Figure 5.

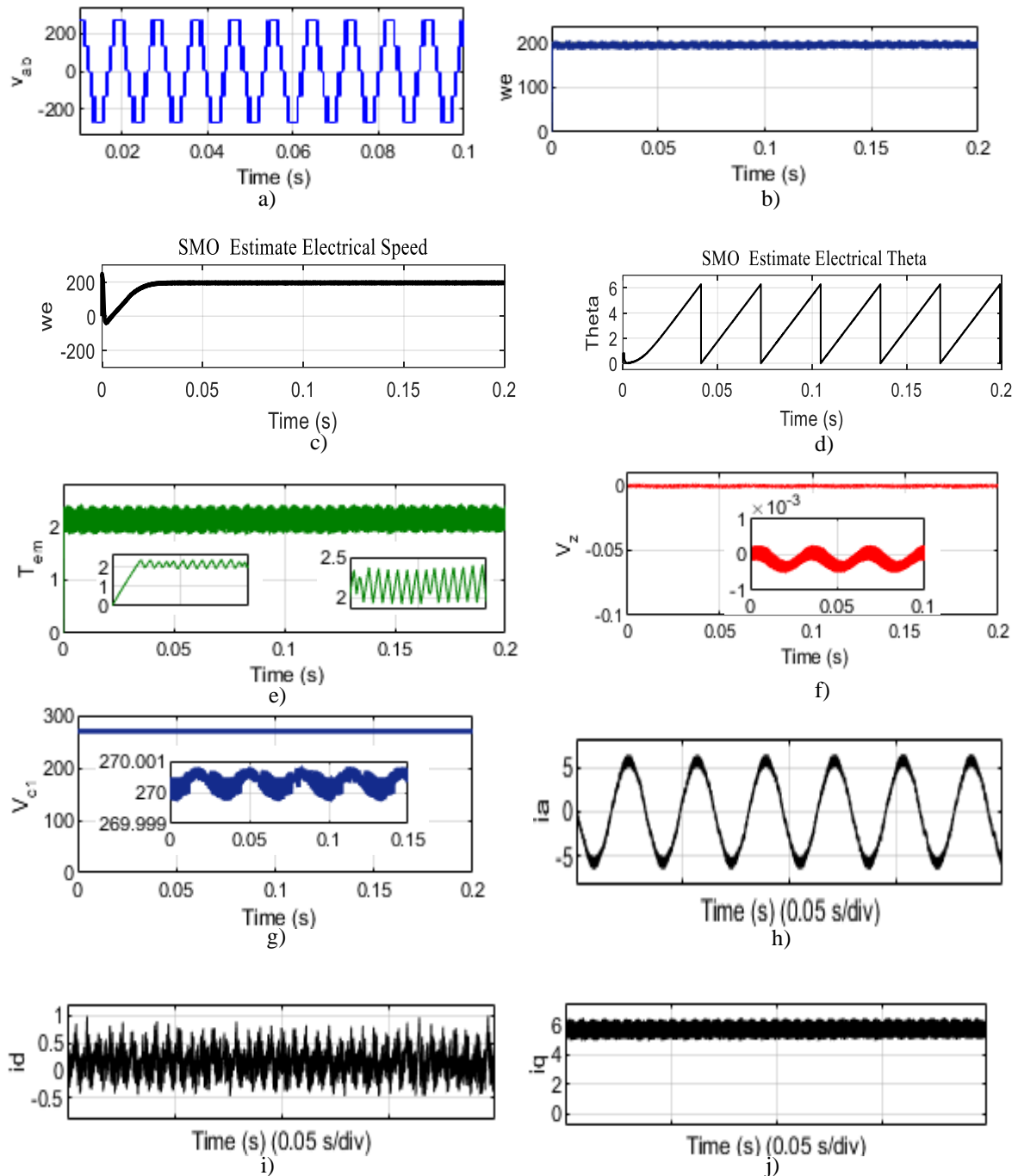


Figure 5. a) Inverter voltage, b) speed, c) observed speed, d) observed electrical angle, e) electromagnetic torque  $T_{em}$ , f) the neutral point voltage  $V_z$ , g)  $V_{c1}$ , h)  $i_a$ , i)  $i_d$ , j)  $i_q$  at  $T_r = 2 \text{ N.m}$

Figure 6 shows the observed electrical angle superimposed on the measured one.

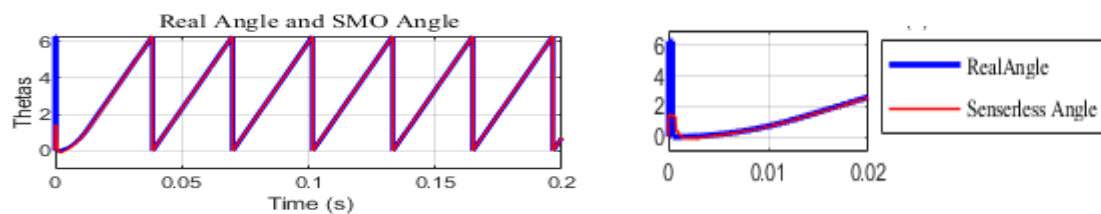


Figure 6. Superposition of the observed and measured angles

For a load torque varying from 2 to 6 N.m in 0.05 s, figure 7 shows the results obtained.

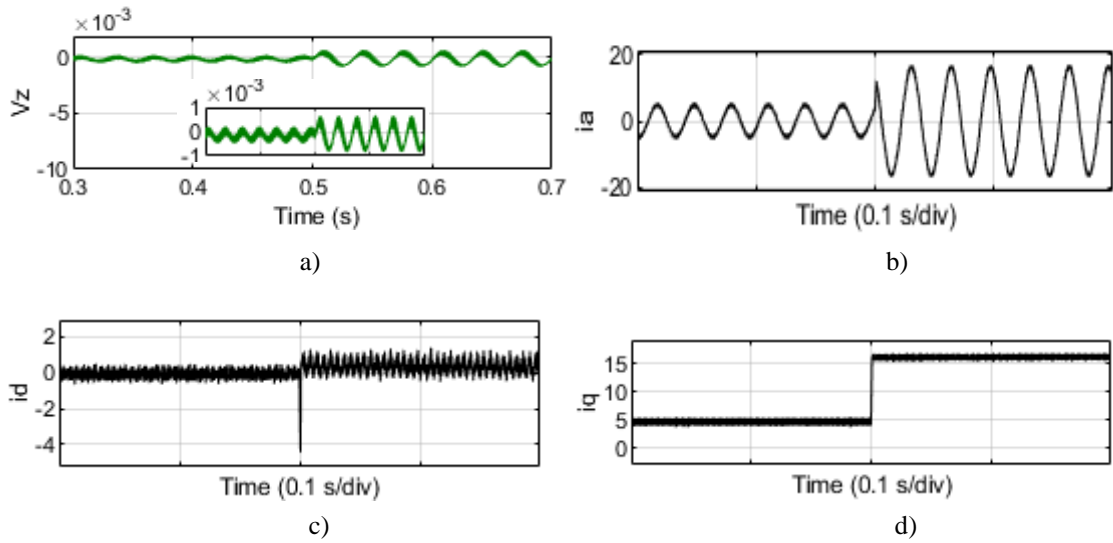


Figure 7. a) Neutral point voltage  $V_z$ , b)  $i_a$ , c)  $i_d$ , d)  $i_q$ , when the load torque varies from 2 N.m to 6 N.m in 0.05 s

To evaluate the transient performance of the control, a simulation test of the reversal of the motor rotation direction is performed. The results are shown in Figure 8 below.

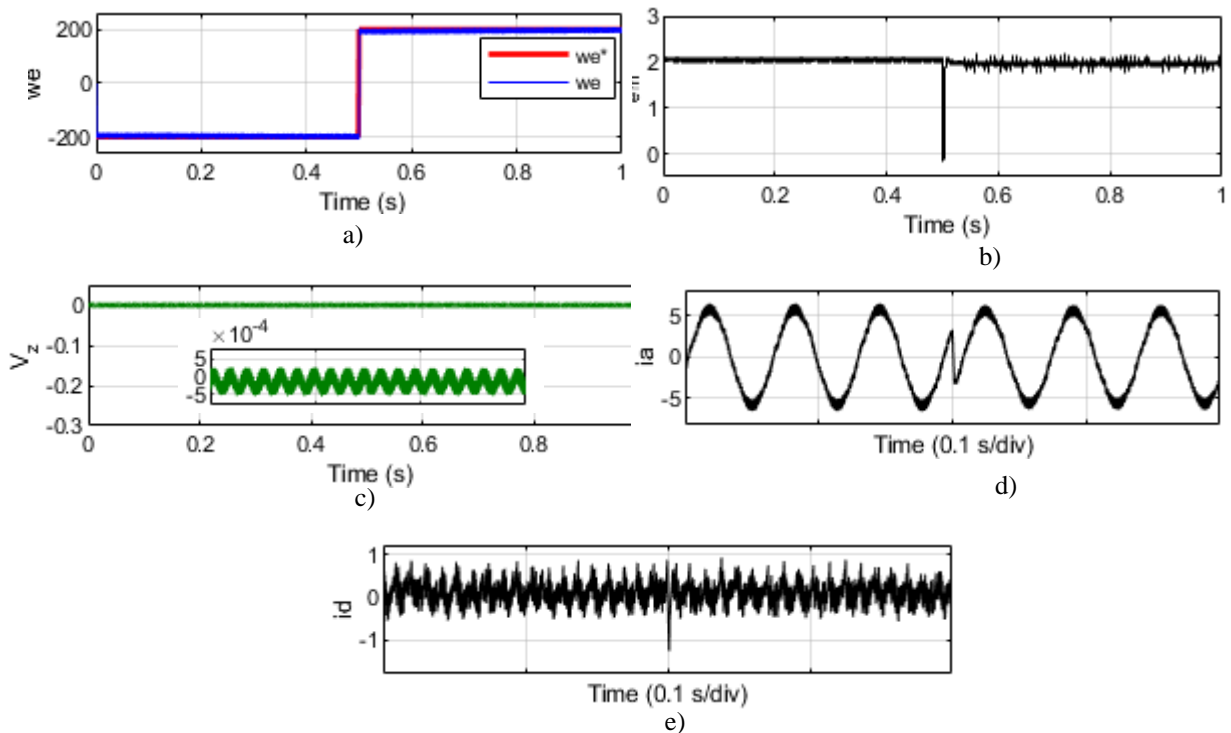


Figure 8. a) Speed, b) electromagnetic torque  $T_{em}$ , c) neutral point voltage  $V_z$ , d)  $i_a$ , e)  $i_d$ .

To further evaluate the transient performance of the control in transient conditions, a simulation test of the engine acceleration is performed. The results are shown in Figure 9 below.

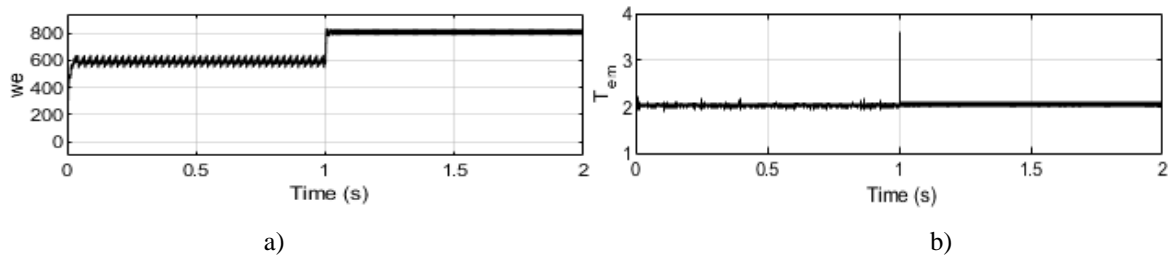


Figure 9. a) Electromagnetic torque, b) speed  $\omega_e$  for acceleration from 600 to 800 rpm

### 3.2. Discussion

From the results shown in Figure 5, it can be seen that the speed  $\omega_e$ , the electromagnetic torque  $T_{em}$ , the current  $i_{c1}$  and the neutral point voltage  $v_z$  are well regulated during constant speed operation. At low load torque, the electromagnetic torque is characterised by small ripples with margins of  $\pm 0.3$  N.m while the inverter neutral point voltage remains very close to 0 with an amplitude of the order of  $10^{-4}$  V. These ripples are thus sufficiently attenuated compared to those obtained by [19] which are about 2.5 N.m and those of [21] which are about 0.4 N.m. The proposed method makes it possible to maintain a constant voltage across capacitors  $C_1$  and  $C_2$  with negligible variations compared to 1 V obtained by [3] or 0.208 V obtained by [11]. It also provides a low harmonic content line current with a THD of 1.69% at 60 Hz for heavy load operation. In this case, there is a considerable decrease in THD compared to the work of [21] where a THD of 9.33% at 27 Hz for a fundamental current of 3.027 A was obtained, that of [10] where a THD of 3.21% was obtained at 40 Hz for a fundamental current of 6.3 A and that of [3] where a THD of 2.12% was obtained for an asynchronous machine. This was achieved by using the 3-level NPC inverter whose output voltage is shown in Figure 5.a) The superposition of the observed rotor angle with that measured by a sensor shown in Figure 6 allows the effectiveness of the sliding mode observer of the rotor speed and electrical angle to be verified. Compared to the work of [14] where the average error is 0.1 rad at 120 rpm, a significant decrease in the estimation error is noticed.

When the load torque is varied from 2 to 6 N.m, Figure 7 shows that the electromagnetic torque reacts positively to the load variation with small ripples but with great dynamics without overshoot. The variations of the voltage at the neutral of the inverter remain controlled as well as the variations of the current  $i_d$  which remain in the vicinity of 0.

Figure 8 shows the ability of the proposed control system to adapt to the reversal of the motor's direction of rotation. Here, the electromagnetic torque is characterised by very good dynamics. It follows its reference perfectly, without overshoot and with a remarkable reduction in ripples. The speed of rotation obtained follows its reference, without any static error and without probable vibration at the machine level since its undulations are lower than 2 rpm for an average speed of 200 rpm. A significant reaction of the current  $i_d$  during the phase of changing the direction of rotation is nevertheless observed. During operation in each direction of rotation, the voltage at the neutral point of the inverter remains around 0.

The feasibility of the proposed method over the conventional FS-MPC studied in [19] is evaluated with the help of Figure 9, which presents the electromagnetic torque and speed in the low speed regime with engine acceleration. While for the conventional FS-MPC the torque ripples remain high in the low speed regime, our method achieves low torque ripples in this speed regime. These ripples are of the order of  $\pm 0.1$  N.m with an overshoot of 10 N.m at the moment of acceleration. This value remains significantly lower than that obtained by [22], which is higher than 12 N.m.

## 4. CONCLUSION

This paper proposes a multi-objective torque predictive control approach for surface-magnetized synchronous motor drives fed by a three-level clamped neutral point inverter. It uses the principle of reducing the number of candidate voltage vectors in the search for the optimal solution and the proportionality between the electromagnetic torque and the current component on the q-axis of the d-q frame to reduce the computational load despite its high number of sub-objectives. A sliding mode observer is used to estimate the motor speed and the angular position of the rotor. It achieves torque and speed control as well as a significant reduction in current harmonics.

## REFERENCES

- [1] Takahashi I, Noguchi T. A new quick-response and high-efficiency control strategy of an induction motor. *IEEE Trans. Ind. Appl.* 1986; 22 (5): 820–827
- [2] Zhang Y, Bai Y. Model Predictive Control of Three-Level Inverter-Fed Induction Motor Drives with Switching Frequency Reduction. *IEEE Trans. Ind. Elec.* 2017; 17(2): 6336–6341
- [3] Osman I, Xiao D, Rahman M. Two-Stage optimization based finite state predictive torque control for 3L-NPC inverter Fed IM drives. *IET Electr. Power. Appl.* 2019; 13(1): 64–72
- [4] Habibullah M, Lu D, Xiao D, Fletcher J E, Rahman M. Low complexity predictive torque control strategies for a three-level inverter driven induction motor. *IET Electr. Power. Appl.* 2017; 11(5): 776–783
- [5] Wang T, Liu W, Lei G, Guo Y, Zhu J. Model predictive direct torque control of permanent magnet synchronous motors with extended set of voltage space vectors. *IET Electr. Power. Appl.* 2017; 11(8):1376–1382
- [6] Bhowate A, Aware M, Sharma S. Predictive Torque Control With Online Weighting Factor Computation Technique to Improve Performance of Induction Motor Drive in Low Speed Region. *IEEE.* 2019; 7: 42309-42321
- [7] Kakosimos P, Abu-Rub H. Predictive Speed Control with Short Prediction Horizon for Permanent Magnet Synchronous Motor Drives. *IEEE Trans. Power. Elec.* 2018; 33(3): 2740–2750
- [8] Mateja N, Haotian X, Tomislav D, Fengxiang W, Jose R, Frede B. Optimal Cost Function Parameter Design in Predictive Torque Control (PTC) Using Artificial Neural Networks (ANN). *IEEE Trans. Power. Elec.* 2020; 68(8): 99–112
- [9] Xia C, Qiu X, Wang Z, Shi T. Predictive torque control for voltage source inverter-permanent magnet synchronous motor based on equal torque effect. *IET Electr. Power Appl.* 2016; 10(3): 208–216
- [10] Katkout A, Nasser T, Essadki A. Robust Multiobjective Model Predictive Control with Computation Delay Compensation for Electric Vehicle Applications Using PMSM with Multilevel Inverter Mathematical Problems in Engineering; 2020
- [11] Xiao D, Akter M P, Alam K, Dutta R, Mekhilef S, Rahman M F. Cascaded Predictive Flux Control for a 3-L Active NPC Fed IM Drives Without Weighting Factor. *IEEE Trans. Energy. Conv.* 2021; 36(3): 1797–1807
- [12] Mahmoud E F, Xu W, El-Sousy F, Islam M R, Ahmed A. Recent Achievements in Model Predictive Control Techniques for Industrial Motor: A Comprehensive State-of-the-Art. *IEEE.* 2021; 9: 58170–58191
- [13] Ezzat M, De Leon J, Glumineau A. Sensorless Speed Control of PMSM via Adaptive Interconnected Observer. *International Journal of Control.* 2011; 84(11): 1926–1943
- [14] Bıçak A., Gelen A. Sensorless direct torque control based on seven-level torque hysteresis controller for five-phase IPMSM using a sliding-mode observer. *Engineering Science and Technology an International Journal.* 2021; 24(6): 1134–1143
- [15] Chen S, Zhang X, Wu X, Tan G, Chen X. Sensorless control for IPMSM based on adaptative super-twisting sliding-mode observer and improved phase-locked loop. *Energies.* 2019; 12(7)
- [16] Zhang X, Foo G, Tung N. Predictive Torque Control of Three-level Sparse Neutral Point Clamped Inverter fed IPMSM Drives using Simplified Deadbeat Principle. *IOP Conf. Earth. Environ. Sci.* 2019
- [17] Jun E, Nguyen M, Kwak S. Three-Phase Three-Level Neutral Point Clamped Rectifier with Predictive Control Method without Employing Weighting Factor. *Applied Sciences.* 2020; 10(15)
- [18] Habibullah M. Simplified Finite-State Predictive Torque Control Strategies for Induction Motor Drives. PhD thesis. University of Sydney; 2016
- [19] Peng S, Zhang G, Zhou Z, Gu X, Xia C. MPTC of NP-clamped three-level inverter-fed permanent-magnet synchronous motor system for NP potential imbalance suppression. *IET Electr. Power. Appl.* 2020; 14(4): 658–667
- [20] Colak I, Kabalci E, Bayindir R. Review of multilevel voltage source inverter topologies and control schemes. *Energy Conversion and Management.* 2011; 52(2): 1114–1128
- [21] Sandre-Hernandez O, Rangel-Magdaleno J, Morales-Caporal R. Modified model predictive torque control for a PMSM-drive with torque ripple minimization. *IET Power. Electron.* 2019; 12(5): 1033–1042
- [22] Xu Y, Hou Y, Li Z. Robust Predictive Speed Control for SPMSM Drives Based on Extended State Observers. *Journal of Power Electronics.* 2019; 19(2): 497–508